Inorganic Chemistry

Article

pubs.acs.org/IC

Structure and Catalytic Activity of Cr-Doped $BaTiO_3$ Nanocatalysts Synthesized by Conventional Oxalate and Microwave Assisted Hydrothermal Methods

Chilukoti Srilakshmi,*[,†] Rohit Saraf,[†] V. Prashanth,[†] G. Mohan Rao,[‡] and C. Shivakumara[†]

[†]Solid State and Structural Chemistry Unit (SSCU) and [‡]Department of Instrumentation and Applied Physics, Indian Institute of Science (IISc), Bangalore, Karnataka, India, 560012

Supporting Information

ABSTRACT: In the present study synthesis of $BaTi_{1-x}Cr_xO_3$ nanocatalysts ($x = 0.0 \leq x \leq 0.05$) by conventional oxalate and microwave assisted hydrothermal synthesis methods was carried out to investigate the effect of synthesis methods on the physicochemical and catalytic properties of nanocatalysts. These catalysts were thoroughly characterized by X-ray diffraction (XRD), Fourier transform infrared spectroscopy (FT-IR), transmission electron microscopy (TEM), X-ray photoelectron spectroscopy (XPS), N_2 physisortion, and total acidity by pyridine adsorption method. Their catalytic performance was evaluated for the reduction of nitrobenzene using hydrazine hydrate as the hydrogen source. Structural parameters refined by Rietveld analysis using XRD powder data indicate that $BaTi_{1-x}Cr_xO_3$ conventional catalysts were crystallized in the tetragonal $BaTiO_3$ structure with space group *P4mm*, and microwave catalysts crystallized in pure cubic $BaTiO_3$ structure with space group $Pm\bar{3}m$. TEM analysis of the catalysts reveal spherical morphology of the particles, and these are uniformly dispersed in microwave catalysts whereas agglomeration of the particles was observed in conventional catalysts. Particle size of the microwave catalysts is found to be 20−35 nm compared to conventional catalysts (30−48 nm). XPS studies reveal that Cr is present in the 3+ and 6+ mixed valence state in all the catalysts. Microwave synthesized catalysts showed a 4−10-fold increase in surface area and pore volume compared to conventional catalysts. Acidity of the $BaTiO_3$ catalysts improved with Cr dopant in the catalysts, and this could be due to an increase in the number of Lewis acid sites with an increase in Cr content of all the catalysts. Catalytic reduction of nitrobenzene to aniline studies reveals that $BaTiO_3$ synthesized by microwave is very active and showed 99.3% nitrobenzene conversion with 98.2% aniline yield. The presence of Cr in the catalysts facilitates a faster reduction reaction in all the catalysts, and its effect is particularly notable in conventional synthesized catalysts.

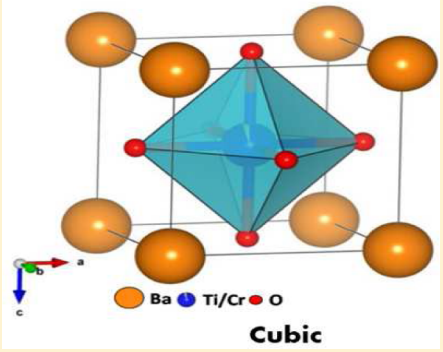

1. INTRODUCTION

In recent years, perovskite-type (ABO_3 structure) transition metal oxides have attracted much attention as catalytic materials due to their thermal and chemical stability, high resistance to dissolution in aqueous and nonaqueous solutions, and cost-effectiveness as compared to noble metals.[1] In ABO_3 structure, A and B are two cations with A atoms larger than B atoms. The chemical properties of the perovskite materials are also known for their flexible characteristics which are associated with their B site substitution capabilities and availability of a wide variety of substoichiometric structures.[2] $BaTiO_3$ (BTO) is an attractive dielectric, ferroelectric, pyroelectric, and electrochemical material for piezo-sensors transducers, infrared sensors, data storage, and tunable microwave dielectric applications.[3−6] The physicochemical properties of $BaTiO_3$ can be improved by doping various transition metals into the lattice.[7] In the present study we have investigated the effect of Cr dopant on the physical and chemical properties of $BaTiO_3$ catalyst synthesized by conventional oxalate and microwave assisted hydrothermal syntheses.

Generally the conventional method of synthesis of perovskites requires conductive heating for extended periods at elevated temperatures leading to large particle size formation, loss of chemical homogeneity, and low sinterability.[8] In order to circumvent this limitation, there is increasing demand for new synthesis methods. The microwave-assisted hydrothermal process is an active area of research in recent years, and this process has been used for the rapid synthesis of numerous ceramic oxides, hydroxylated phases, porous materials, and metal powders.[9−11] It offers several advantages in comparison to conventional heating such as fast crystallization, cost efficiency, and clean technology, and furthermore it is energy efficient and economical. In the present investigation, we have achieved considerable reduction in time required for the synthesis of perovskites of $BaTi_{1-x}Cr_xO_3$ ($x = 0.5$, 2.5, and 5 mol %) using this methodology and compared the physicochemical and catalytic properties of these catalysts with those prepared by a conventional oxalate method of synthesis. All the catalysts synthesized via both the methods were evaluated for catalytic reduction of nitrobenzene to aniline.

Aniline is widely used in the chemical industries as intermediates for the production of dyes, pharmaceuticals, plastics (especially polyurethanes), herbicides, and pigments.[12,13] Generally, aniline is

Received: January 29, 2016

DOI: 10.1021/acs.inorgchem.6b00240
Inorg. Chem. XXXX, XXX, XXX−XXX

manufactured through the reduction of nitrobenzene (NB) via catalytic reduction in liquid or gas phase and metallic reagents in acidic media. Numerous methods containing homogeneous catalytic reduction and heterogeneous catalytic reduction have been reported in the literature for the reduction of nitroarenes to anilines. Recently, catalytic reduction using homogeneous complexes of Pd, Fe, Cu, Ni, and Fe[14−17] with 2-propanol as hydrogen donor has gained much attention. But reduction rates are considerably low with these catalysts and involve various problems such as deactivation by metal precipitation or ligand degradation and separation difficulties, etc. On the other hand, the use of heterogeneous catalysts offers several advantages over homogeneous systems with respect to easy recovery and recycling of the catalysts as well as minimization of undesired toxic wastes. In the present paper we present the results of catalytic reduction of nitro compounds over Cr-doped $BaTiO_3$ perovskite. Perovskites have been used previously for the decomposition of NO_x[18] oxidation of CO[19] and NH_3.[20] However, their application for the reduction of nitro aromatics to amino aromatics without side reactions has been scarcely studied and remains a challenging task. In our previous papers, we have presented various transition metal doped $BaTiO_3$ and the effect of dopant on catalytic reduction of nitrobenzene to azoxybenzene.[21] Chromium-doped metal oxides has been primarily studied for resistance-change memory,[22] photocatalysis,[23] oxygen gas sensor,[24] and reduction of NO;[25] its reactivity for nitrobenzene reduction remains relatively unexplored. In this context, we have explored Cr-doped $BaTiO_3$ catalysts for the selective reduction of nitrobenzene to aniline. The catalysts were characterized using powder X-ray diffraction (XRD), Fourier transform infrared (FTIR) spectroscopy, transmission electron microscopy (TEM), X-ray photoelectron spectroscopy (XPS), N_2 physisorption and acidity by the pyridine adsorption method.

2. EXPERIMENTAL SECTION

2.1. Materials. Barium nitrate ($Ba(NO_3)_2$), barium chloride dihydrate ($BaCl_2{\cdot}2H_2O$), titanium isopropoxide ($Ti(OC_3H_7)_4$), titanium tetrachloride ($TiCl_4$), chromium nitrate nonahydrate ($Cr(NO_3)_3{\cdot}9H_2O$), oxalic acid ($C_2H_2O_4{\cdot}2H_2O$), potassium hydroxide (KOH), 2-propanol (C_3H_7OH), and hydrazine hydrate ($N_2H_4{\cdot}H_2O$) used in the experiments were purchased from Sigma-Aldrich and Merck. All reagents are of analytical purity and were used without further purification.

2.2. Synthesis of $BaTiO_3$ and Cr-Doped $BaTiO_3$ Nanocatalysts. *2.2.1. Conventional Oxalate Method (CO).* $BaTiO_3$ and Cr-doped $BaTiO_3$ nanocatalysts were synthesized by a conventional oxalate route as follows: Stoichiometric amounts of titanium isopropoxide, barium nitrate, and chromium nitrate as metal oxide precursors, and oxalic acid as chelating agent were used as raw materials. These materials were mixed in a molar ratio of $Ti(OC_3H_7)_4$: $Ba(NO_3)_2$: $C_2H_2O_4{\cdot}2H_2O$ = 1:1:2 in a mixture of 2-propanol and water. A homogeneous solution was obtained after stirring at 60 °C for 1 h. Then the solution was evaporated to dryness at 100 °C. The oxalate precursors thus obtained were dried in hot air oven at 120 °C for overnight. The dried precursors obtained were ground to fine powders and calcined at 900 °C for 12 h. For Cr substituted $BaTiO_3$ catalysts, a similar method was followed except the stoichiometric addition of chromium nitrate to the above solution in the following ratio $Ba(NO_3)_2$: $1-x$$Ti(OC_3H_7)_4$: $x$$Cr(NO_3)_3{\cdot}9H_2O$: $C_2H_2O_4{\cdot}2H_2O$ where $x = 0.0 \leq x \leq 0.05$ respectively.

2.2.2. Microwave-Assisted Hydrothermal Method (MH). In microwave-assisted hydrothermal method, barium chloride dihydrate, titanium tetrachloride, chromium nitrate nonahydrate, and potassium hydroxide were chosen as starting materials. The molar ratio of $BaCl_2{\cdot}2H_2O$: $TiCl_4$: Cr $(NO_3)_3{\cdot}9H_2O$: KOH: H_2O was 2: $(1-x)$: x: 30:300. Initially $TiCl_4$ was added to the required amount of water at 0 °C. $BaCl_2{\cdot}2H_2O$, Cr $(NO_3)_3{\cdot}9H_2O$, and KOH were separately dissolved in deionized water and added to the $TiCl_4$ solution and stirred for 30 min. The resultant mixture was transferred into Teflon-lined autoclave, sealed, and placed in microwave instrument at 180 °C for 30 min (MW 5000, *SINEO*, maximum power of 1500 W). After the reaction, the autoclave was cooled to room temperature. The solid product was washed with 0.1 M aqueous acetic acid solution and deionized water. The final product was recovered with centrifugation and dried in a hot air oven at 105 °C overnight. Pure $BaTiO_3$ was prepared in the same way but without addition of chromium nitrate. The list of catalysts synthesized by the conventional oxalate and microwave method is given in Table 1.

Table 1. List of $BaTiO_3$ and Cr-Doped $BaTiO_3$ Catalysts Synthesized by the Conventional Oxalate and Microwave Method and Their Average Crystallite Size Calculated from XRD

catalyst name	catalyst notation	average crystallite size
$BaTiO_3$ (conventional oxalate (CO))	BTO_1	50.9
0.5 mol % Cr-doped $BaTiO_3$ (CO)	BTO_2	54.8
2.5 mol % Cr-doped $BaTiO_3$ (CO)	BTO_3	58.7
5 mol % Cr-doped $BaTiO_3$ (CO)	BTO_4	63.5
$BaTiO_3$ (microwave hydrothermal (MH))	BTO_5	32.8
0.5 mol % Cr-doped $BaTiO_3$ (MH)	BTO_6	37.3
2.5 mol % Cr-doped $BaTiO_3$ (MH)	BTO_7	39.5
5 mol % Cr-doped $BaTiO_3$ (MH)	BTO_8	45.8

2.3. Characterization Techniques. Powder X-ray diffraction (XRD) patterns of the catalysts were recorded using a PANanalytical X'pert PRO powder diffractometer with Cu Kα (λ = 1.5418 Å) as the radiation source. Rietveld analysis measurement was performed in a step mode with 2θ varying from 10° to 80° with a scanning rate of 0.02° min^{-1}. The structural parameters were estimated by using the Full Prof Suite-2000 program. Fourier transform infrared (FTIR) spectra of catalysts were measured on a PerkinElmer FTIR-300 spectrometer using a KBr pellet method. The transmission electron microscopy (TEM) analysis was performed on a JEOL 2100F electron microscope with an acceleration voltage of 200 kV. The Brunauer−Emmett−Teller (BET) surface area of the samples was measured using a Model-Quantachrome Autosorb iQ2 automated gas sorption analyzer. Samples were initially pretreated in N_2 at 300 °C for 4 h, and the BET surface area and pore volume of the catalysts were obtained by adsorbing N_2 at liquid nitrogen temperature, −196 °C. X-ray photoelectron spectra (XPS) were recorded on an ESCA-3 Mark II spectrometer (VG Scientific Ltd., England) using Al Kα radiation (1486.6 eV). Binding energies were calculated with respect to C (1 s) at 285 eV and measured with a precision of ±0.2 eV. Acidity measurements were conducted using pyridine as a probe molecule using FTIR spectroscopy. Catalyst samples were activated by degassing at 120 °C for 2 h and then saturated with pyridine. The samples were then evacuated at 115 °C for 60 min to remove physisorbed pyridine. FT-IR spectra of the samples were then recorded in the range of 1400−1600 cm^{-1} using a PerkinElmer FTIR-300 spectrometer having a resolution of 4 cm^{-1} with 60 scans.[26,27]

2.4. Catalytic Activity. Catalytic reduction with hydrazine hydrate as a hydrogen donor was carried out under continuous stirring in a two-necked 100 mL round-bottom flask fitted with a reflux condenser. Analysis was done by withdrawing definite aliquots of the reaction sample at regular intervals. In a typical run, 80 mg of the catalyst was dispersed in a solution containing 10 mmol of nitrobenzene, 10 mmol of KOH pellets, and 10 mL of 2-propanol. The mixture was stirred and heated under reflux at 80 °C for 2−6 h in an oil bath. GC−MS analysis of the product samples was carried out using Thermo Trace GC Ultra (GC), Thermo DSQ II (MS); with DB5 MS column of 30 m L × 0.25 mm ID × 0.25 μm film thickness and with Electron Multiplier detector.

3. RESULTS AND DISCUSSION

3.1. Powder X-ray Diffraction. BTO and Cr-doped BTO powders synthesized by above-mentioned two methods have been analyzed by XRD studies. XRD patterns of the Cr-doped $BaTiO_3$

DOI: 10.1021/acs.inorgchem.6b00240
Inorg. Chem. XXXX, XXX, XXX−XXX

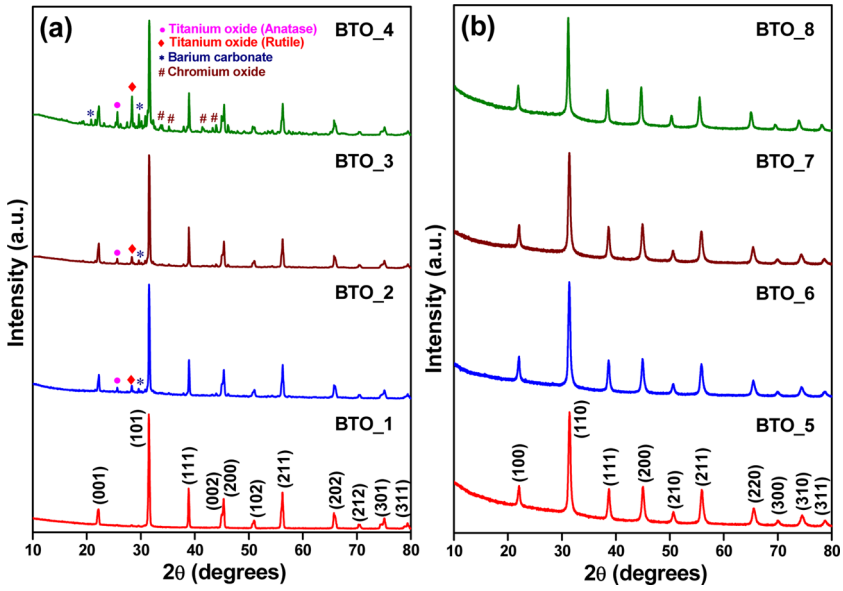

Figure 1. Powder XRD patterns of $BaTiO_3$ and Cr-doped $BaTiO_3$ catalysts synthesized using (a) CO method and (b) MH method.

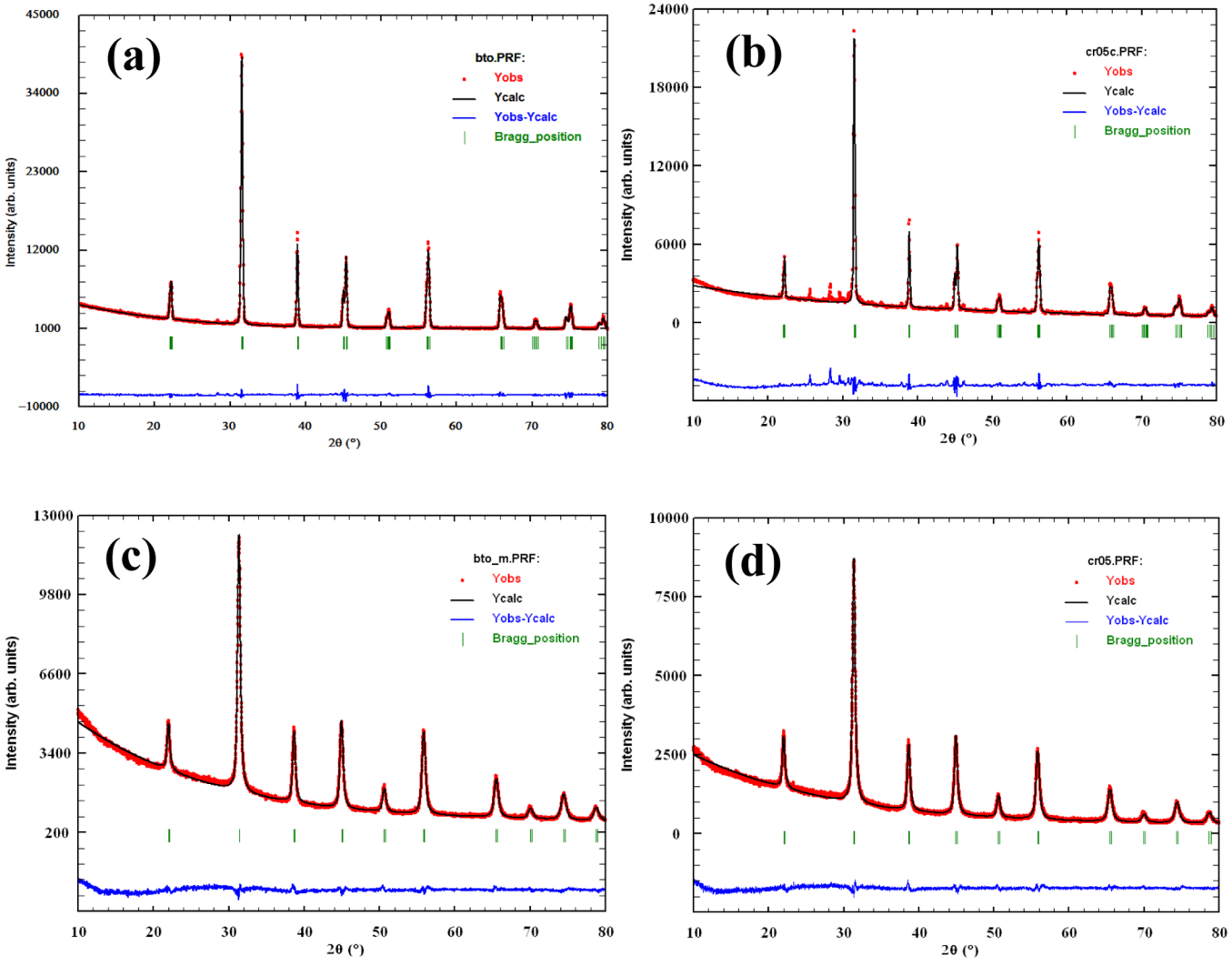

Figure 2. Observed, calculated, and difference XRD patterns of (a) BTO_1, (b) BTO_2, (c) BTO_5, and (d) BTO_6.

(0.5, 2.5, and 5 mol %) powders synthesized by the CO method and heat treated at 900 °C showed a similar XRD pattern (Figure 1a) as that of pure BTO which illustrates the splitting of diffraction peaks at $2\theta \approx 45°$ corresponds to (002) and (200) planes of

DOI: 10.1021/acs.inorgchem.6b00240
Inorg. Chem. XXXX, XXX, XXX−XXX

tetragonal phase with space group *P4mm* (No. 99) of $BaTiO_3$ (JCPDS card no. 079-2265). Trace amounts of titanium oxide, barium carbonate, and chromium oxide were observed as impurities in Cr-doped BTO catalysts.

The XRD patterns of as-synthesized catalysts by the MH method (Figure 1b) illustrate the absence of apparent splitting at $2\theta \approx 45^\circ$ corresponds to the tetragonal phase indicating the presence of pure cubic crystalline phase of $BaTiO_3$ with space group $Pm\bar{3}m$ (No. 221) (JCPDS card no. 075-0213). No trace of impurities has been observed in the XRD patterns of the catalysts. This implies that the chromium ion substituted to six coordinated titanium ions in a $BaTiO_3$ lattice. This reveals that a monophasic system was obtained using a microwave-assisted hydrothermal method.

The average crystallite size was calculated using Scherrer formula:

$$D = \frac{0.9\lambda}{(B^2 - b^2)^{1/2} \cos\theta} \quad (1)$$

where D is the average crystallite size, λ is the X-ray wavelength, θ is the Bragg angle, and B and b are the full width at half maxima (fwhm) observed for the sample and standard, respectively. The average crystallite size evaluated from XRD patterns is given in Table 1. The average crystallite size of the MH synthesized catalysts is less as compared to CO catalysts, and it was observed that the crystallite size of Cr-doped BTO catalysts increased with the increase in Cr concentration in both CO and MH synthesized catalysts. This could be due to the substitution of higher radii Cr ion to the lower radii Ti ionic site in the $BaTiO_3$ host lattice.[28] From these results, it was proposed that the successful synthesis of pure Cr-doped BTO nanocatalysts without any impurities and having less crystallite size and good dispersion obtained with MH method was attributed to the rapid microwave heating.

3.2. Structural Parameters Estimation by Rietveld Refinement Analysis. The crystal structure and lattice parameters have been evaluated by the Rietveld refinement method using powder XRD data of the catalysts in the FullProf program. The patterns were typically refined for lattice parameters, scale factor, backgrounds, pseudo-Voigt profile function (u, v, and w), atomic coordinates and isothermal temperature factors (B_{iso}). In order to distinguish between the cubic and tetragonal phases, the commonly used characteristic peak in the diffraction pattern, ranges between $2\theta = 40-50^\circ$ region, where the single cubic (200) peak splits into two tetragonal peaks (002) and (200). Figure 2 and Figure S1 illustrate the observed, calculated, and difference XRD patterns of $BaTiO_3$ Cr-doped $BaTiO_3$ catalysts. There is a good agreement between experimentally observed and calculated XRD patterns ($Y_{obs} - Y_{cal}$ is close to zero), which is based on the consideration of relatively lower R_p and R_{wp} (<10%) values. The refinement result confirmed that the compounds synthesized using CO method has tetragonal structure, whereas MH synthesized compounds belong to cubic symmetry. The lattice parameters, cell volume, space group, atomic positions, and R-values obtained after Rietveld refinement process, for $BaTiO_3$ and Cr-doped $BaTiO_3$ catalysts synthesized using conventional oxalate and microwave method are summarized in Table 2 and Table 3, respectively. As expected the cell volume of cubic $BaTiO_3$ catalysts is more than a tetragonal phase. The increase in lattice parameters and cell volume with an increase in Cr doping content (up to 5 mol %) confirmed that Cr ions substituted Ti ions in the $BaTiO_3$ host lattice.

Table 2. Rietveld Refined Structural Parameters and Unit Cell Volumes for $BaTiO_3$ and Cr-Doped $BaTiO_3$ Catalysts Synthesized Using Conventional Oxalate Method

catalysts	BTO_1	BTO_2	BTO_3	BTO_4
crystal system	tetragonal	tetragonal	tetragonal	tetragonal
space group	*P4mm* (No. 99)	*P4mm* (No. 99)	*P4mm* (No. 99)	*P4mm* (No. 99)
lattice parameters				
a (Å)	3.9968(1)	3.9993(3)	3.9996(3)	4.0003(5)
b (Å)	3.9968(1)	3.9993(3)	3.9996(3)	4.0003(5)
c (Å)	4.0280(1)	4.0274(5)	4.0285(4)	4.0320(1)
cell volume (Å^3)	64.345(3)	64.418(1)	64.451(1)	64.521(3)
atomic positions				
Ba (1a)				
x	0.0000	0.0000	0.0000	0.0000
y	0.0000	0.0000	0.0000	0.0000
z	0.0000	0.0000	0.0000	0.0000
Ti/Cr (1b)				
x	0.5000	0.5000	0.5000	0.5000
y	0.5000	0.5000	0.5000	0.5000
z	0.5243(2)	0.5283(7)	0.5222(8)	0.5323(1)
O1 (1b)				
x	0.5000	0.5000	0.5000	0.5000
y	0.5000	0.5000	0.5000	0.5000
z	0.0326(5)	0.0521(2)	0.0182(5)	0.0469(6)
O2 (2c)				
x	0.5000	0.5000	0.5000	0.5000
y	0.0000	0.0000	0.0000	0.0000
z	0.4892(8)	0.5189(4)	0.5192(2)	0.5148(4)
$R_{Factors}$ (%)				
R_p	2.94	5.83	8.29	11.7
R_{wp}	4.16	7.76	11.2	15.3
R_{exp}	2.27	2.78	1.34	1.38
R_{Bragg}	2.59	9.30	10.7	22.3
R_F	2.26	4.33	7.64	12.7
χ^2	3.37	7.79	70.3	123.1

As shown in Table 2, the lattice parameters of BTO with the space group *P4mm* are $a = b = 3.9968(1)$ Å, and $c = 4.0280(1)$ Å, which are close to the published lattice parameters: $a = b = 3.9990(1)$ Å, and $c = 4.0180(2)$ Å (JCPDS card No. 079-2265). The lattice parameters found for BTO with the space group $Pm\bar{3}m$ (Table 3) are also close to the published data: $a = b = c = 4.0335(3)$ Å (JCPDS card No. 075-0213). In the cubic $BaTiO_3$ perovskite structure, the Ba atoms are in the Wyckoff position 1a, (0, 0, 0); the Ti atoms in 1b, (0.5, 0.5, 0.5); and the O atoms in 3c (0.5, 0, 0.5), all special positions. In the tetragonal unit cell, atoms are displaced in the z-direction, and the cell is elongated along the c-axis. Atom positions and Wyckoff position for tetragonal $BaTiO_3$ perovskite are Ba (1a) at (0, 0, 0); Ti (1b) at (0.5, 0.5, z); O1 (1b) at (0.5, 0.5, z); and O2 (2c) at (0.5, 0, z).

The crystal structure of $BaTiO_3$ and Cr-doped $BaTiO_3$ was modeled using Rietveld refined structural parameters by the VESTA program. In cubic $BaTiO_3$, the structure of which is displayed in Figure 3a, the large barium atom is located at eight corners, the smaller titanium atom sitting in the body center, and the oxygen atom in the face center. The resulting perovskite structure can also be described as consisting of corner sharing $[TiO_6]$ octahedra with the Ba^{2+} ion occupying the 12-fold coordination site formed in the middle of the cube of eight such octahedral, as shown in Figure 3b. The bond length of all six Ti−O bonds is 2.0146 Å. Similarly in the 5 mol % Cr-doped

DOI: 10.1021/acs.inorgchem.6b00240
Inorg. Chem. XXXX, XXX, XXX−XXX

Table 3. Rietveld Refined Structural Parameters and Unit Cell Volumes for $BaTiO_3$ and Cr-Doped $BaTiO_3$ Catalysts Synthesized Using Microwave Method

catalysts	BTO_5	BTO_6	BTO_7	BTO_8
crystal system	cubic	cubic	cubic	cubic
space group	$Pm\bar{3}m$ (No. 221)	$Pm\bar{3}m$ (No. 221)	$Pm\bar{3}m$ (No. 221)	$Pm\bar{3}m$ (No. 221)
lattice parameters				
a (Å)	4.0292(3)	4.0311(3)	4.0362(2)	4.0546(3)
b (Å)	4.0292(3)	4.0311(3)	4.0362(2)	4.0546(3)
c (Å)	4.0292(3)	4.0311(3)	4.0362(2)	4.0546(3)
cell volume (Å^3)	65.410(1)	65.506(1)	65.752(1)	66.657(1)
atomic positions				
Ba (1a)				
x	0.0000	0.0000	0.0000	0.0000
y	0.0000	0.0000	0.0000	0.0000
z	0.0000	0.0000	0.0000	0.0000
Ti/Cr (1b)				
x	0.5000	0.5000	0.5000	0.5000
y	0.5000	0.5000	0.5000	0.5000
z	0.5000	0.5000	0.5000	0.5000
O (3c)				
x	0.5000	0.5000	0.5000	0.5000
y	0.0000	0.0000	0.0000	0.0000
z	0.5000	0.5000	0.5000	0.5000
$R_{Factors}$ (%)				
R_p	3.01	3.84	3.82	3.40
R_{wp}	3.66	4.77	4.70	4.22
R_{exp}	2.29	3.11	3.08	2.29
R_{Bragg}	6.08	2.76	3.15	7.93
R_F	2.47	1.57	1.65	3.36

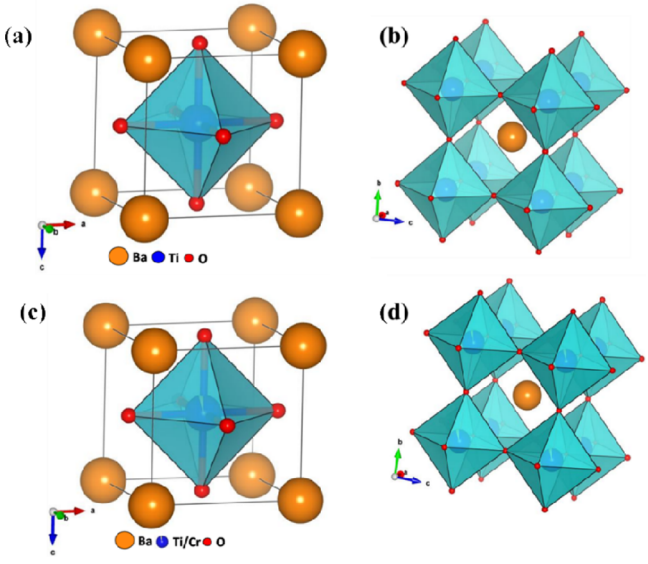

Figure 3. Cubic unit cell of (a) BTO_1, (c) BTO_4 and crystal structure of (b) BTO_1, (d) BTO_4.

$BaTiO_3$ compound, the chromium atom substitutes for the titanium atom and is also bonded to six oxygen atoms (Figure 3c,d).

The ideal cubic perovskite structure is not very common and is slightly distorted. The distortion of the [TiO_6] octahedra may be due to temperature changes or stress effects that lead to the transition from cubic structure to tetragonal. Three main factors are identified as being the possible reason for the distortion in perovskite structure: size effects of atoms, deviations from ideal

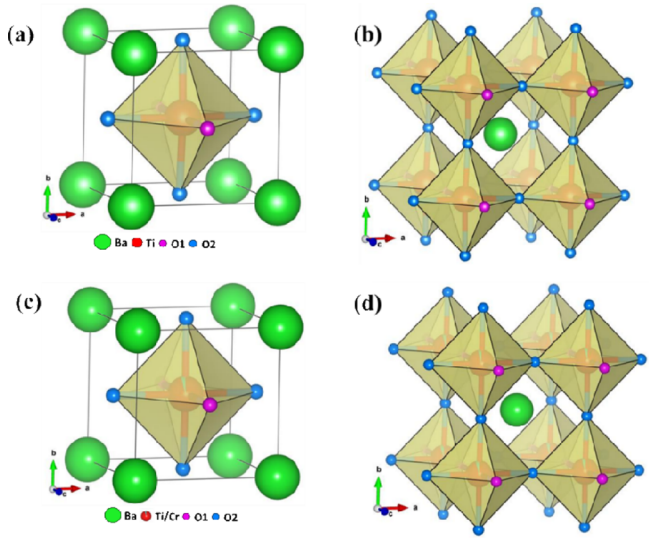

Figure 4. Tetragonal unit cell of (a) BTO_5, (c) BTO_8 and crystal structure of (b) BTO_5, (d) BTO_8.

composition, and the Jahn–Teller effect.[29] In the tetragonal $BaTiO_3$ structure (Figure 4a), the barium atom is also located at eight corners, titanium atom at body center, and oxygen atom at six face centers. The titanium atom coordinated to six oxygen (O) atoms having two types of Ti–O distances. Out of six Ti–O bonds, two are Ti–O1 with bond length 2.0474 Å, and four are Ti–O2 with bond length 2.0034 Å. The resulting crystal structure is shown in Figure 4b. Similarly for the 5 mol % Cr-doped $BaTiO_3$ compound (Figure 4c,d), the chromium atom substitutes for the titanium atom and is also bonded to six oxygen atoms.

3.3. FT-IR Spectroscopy. FT-IR spectra of $BaTiO_3$ and Cr-doped $BaTiO_3$ catalysts synthesized by the conventional oxalate and microwave method are shown in Figure 5. The IR bands observed in the range between 395 and 420 cm^{-1} correspond to characteristic TiO_{II} bending vibrations. The broad absorption band at 560–620 cm^{-1} is ascribed to TiO_{VI} stretching vibration connected to the barium.[30] The band situated at 855–880 cm^{-1} can be assigned to metal–oxygen stretching vibrations.[21] In Figure 5a, the band at 1365 cm^{-1} observed for the BTO_4 sample can be attributed to the vibrational mode of CO_3^{2-} group, indicating the presence of barium carbonate ($BaCO_3$) impurity in the catalysts.

3.4. Morphological Analysis. The morphology and particle size of $BaTiO_3$ and Cr-doped $BaTiO_3$ catalysts were studied by transmission electron microscopy. As shown in Figure 6a–f, the particles are spherical in shape in all the catalysts. In CO synthesized $BaTiO_3$, (Figure 6a) the agglomerated particles are observed, whereas the MH synthesized $BaTiO_3$ (Figure 6b) particles are dispersed due to the uniform microwave heating which lead to molecular agitation and hence resist the particles agglomeration. The average particle size calculated from TEM images is listed in Table 4. The result reveals that the particle size increases with an increase in Cr content in $BaTiO_3$ in all the catalysts from 30.8 to 47.4 nm using the CO method. However, the particle size of MH synthesized catalysts was observed to be 20.7–34.9 nm, which was less compared to CO synthesized catalysts. The MH method is the best method compared to the CO method by virtue of its simple operation and short reaction times, and it utilizes a cavitation effect to obtain a high heating rate constant and radio frequency heating from inside to outside which induces the creating velocity of the powder much faster than the growing velocity. So the particle size is as small as

DOI: 10.1021/acs.inorgchem.6b00240
Inorg. Chem. XXXX, XXX, XXX–XXX

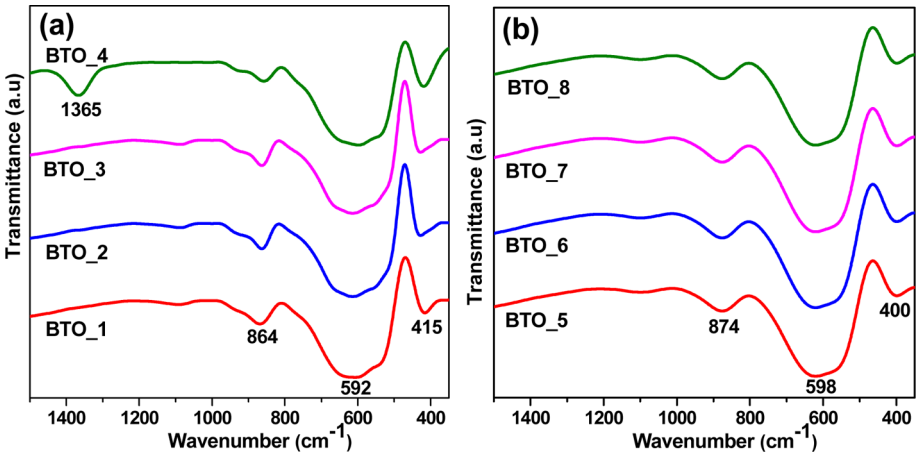

Figure 5. FT-IR spectra of $BaTiO_3$ and Cr-doped $BaTiO_3$ catalysts synthesized using (a) CO method (b) MH method.

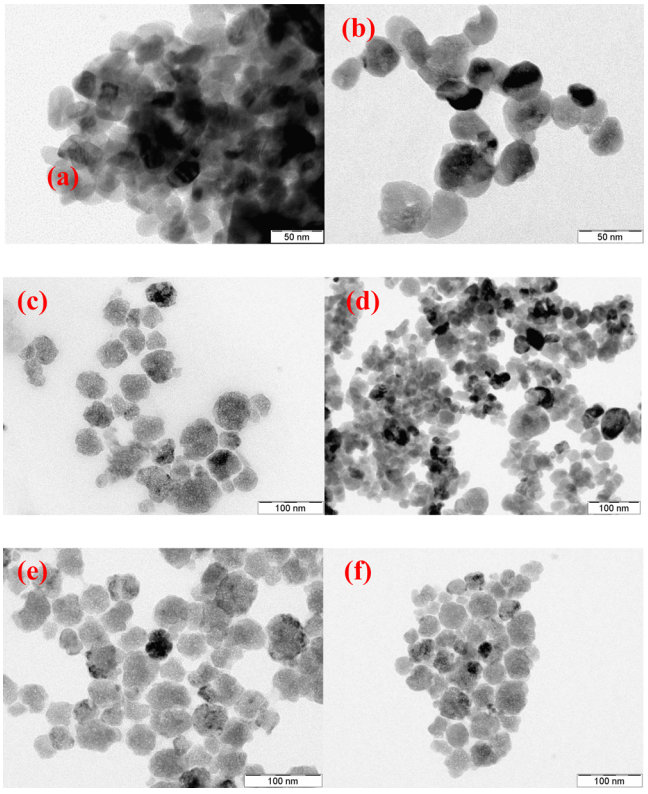

Figure 6. TEM images of $BaTiO_3$ and Cr-doped $BaTiO_3$ catalysts: (a) BTO_1, (b) BTO_5, (c) BTO_3, (d) BTO_7, (e) BTO_4, and (f) BTO_8 catalysts.

40 nm and has a homogeneous distribution.[31] TEM particle size analysis is in good agreement with the calculated XRD crystallite size as both increase with an increase in the Cr content of the catalysts.

Figure 7a,b illustrates the high-resolution TEM images of 2.5 mol % Cr-doped $BaTiO_3$ catalysts. Clear lattice fringes are observed with the measured interplanar spacing values of about 0.283 and 0.285 nm, corresponding to the crystallographic plane (101) of tetragonal $BaTiO_3$ (JCPDS card no. 079-2265, $d_{(101)}$ = 0.283 nm) and the (110) crystal plane spacing of the cubic $BaTiO_3$ phase (JCPDS card no. 075-0213, $d_{(110)}$ = 0.285 nm), respectively. Energy dispersive X-ray (EDX) spectra of $BaTiO_3$ and Cr-doped $BaTiO_3$ catalysts are shown in Figure 7c–e. EDX analysis reveals the presence of Ba, Ti, and O elements in $BaTiO_3$ and further confirmed the presence of the Cr element in Cr-doped $BaTiO_3$ catalysts synthesized by both CO and MH methods.

Table 4. Average Particle Size Determined from TEM Images for $BaTiO_3$ and Cr-Doped $BaTiO_3$ Catalysts

	average particle size (nm)	
catalysts	conventional	microwave
$BaTiO_3$	30.8	20.7
0.5 mol % Cr-doped $BaTiO_3$	38.3	28.0
2.5 mol % Cr-doped $BaTiO_3$	43.6	31.3
5 mol % Cr-doped $BaTiO_3$	47.4	34.9

3.5. BET Surface Area by N_2 Physisorption. The surface area of CO and MH synthesized catalysts are given in Table 5. The surface area of MH synthesized catalysts was increased from 4- to 10-fold, whereas the total pore volume was raised to 10-fold compared to CO synthesized catalysts. This could be due to improvement in porosity of the materials synthesized by the MH method due to uniform heating and faster heating rate throughout the sample compared to the CO method in which heating at elevated temperatures for extended periods led to collapse of pores, and thereby a decrease in surface area and pore volume will take place. It was found that the surface area of 0.5 mol % Cr-doped $BaTiO_3$ catalyst was more compared to pure $BaTiO_3$ in both the CO and MH synthesized catalysts. This could be due to contribution from Cr content of the catalysts. The decrease in surface area of the catalysts at high Cr content (2.5 and 5 mol %) in $BaTiO_3$ was due to formation of larger particles as latter was confirmed with TEM image particle size analysis of the catalysts (Table 4). These results indicate that a perovskite with a high surface area and pore volume having good dispersion of metals in the matrix can be synthesized using microwave technology.

3.6. X-ray Photoelectron Spectroscopy (XPS) Analysis. The representative XPS survey spectrum of 2.5 mol % Cr-doped $BaTiO_3$ CO synthesized catalyst is presented in Figure 8a. It reveals the presence of C, O, Ba, Ti, and Cr elements in the catalyst. The peak at the binding energy of 284.52 eV in survey spectra can be assigned to C 1s which may be due to the presence of CO_2 in the air.[32] Apart from Ba 3d peak, the other Ba 4d and Ba 4p signals observed at 88.52 and 176.78 eV were due to different barium orbitals present in $BaTiO_3$.[32]

Figure 8b illustrates the high-resolution Ba 3d XPS spectra which reveal two peaks at the binding energy of 778.64 and 793.88 eV. These are assigned due to splitting of the Ba $3d_{5/2}$ and Ba $3d_{3/2}$ spin states, and it indicates the oxidation state of Ba is 2+.[33]

DOI: 10.1021/acs.inorgchem.6b00240
Inorg. Chem. XXXX, XXX, XXX−XXX

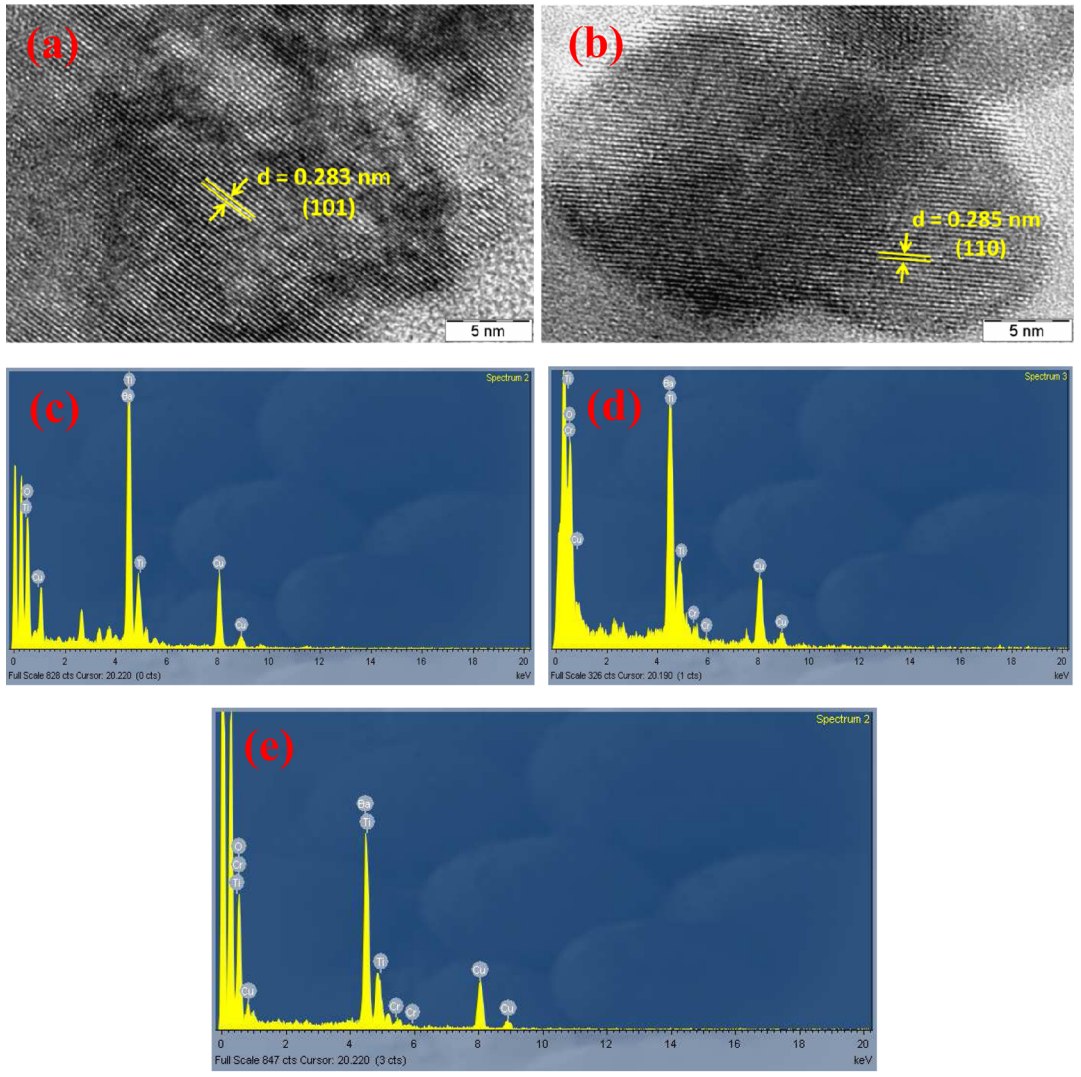

Figure 7. High-resolution TEM images showing the lattice fringes of Cr-doped $BaTiO_3$ catalysts: (a) BTO_3 and (b) BTO_7 and EDX spectra of $BaTiO_3$ and Cr-doped $BaTiO_3$ catalysts: (c) BTO_1, (d) BTO_4 and (e) BTO_7.

Table 5. Physicochemical Properties of Various BTO Catalysts

catalyst	BET surface area (m^2/g)	total pore volume (cc/g)	amount of Lewis acidity (μmol/g)
BTO_1	8.90	2.54×10^{-3}	327
BTO_2	20.5	2.62×10^{-3}	345
BTO_3	17.6	2.56×10^{-3}	371
BTO_4	6.17	2.20×10^{-3}	382
BTO_5	71.4	3.55×10^{-2}	329
BTO_6	84.6	4.02×10^{-2}	347
BTO_7	73.8	3.77×10^{-2}	373
BTO_8	69.6	2.38×10^{-2}	389

The XPS spectra of Ti 2p (Figure 8c) revealed two peaks. The strong peak observed at 458.03 eV was ascribed to Ti $2p_{3/2}$, and the less intense peak at 463.79 eV corresponds to Ti $2p_{1/2}$, both were due to Ti^{4+} oxidation state.[34,35]

XPS spectra of Cr-doped $BaTiO_3$ catalysts (Figure 8d) showed two broad Cr 2p peaks[36] at 578.64 and 589.45 eV. After peak fitting analysis, using Gaussian function the broad peak at 578.64 eV deconvoluted into three peaks at 575.06, 577.85, and 579.95 eV corresponding to Cr $2p_{3/2}$ of the Cr^{3+} and Cr^{6+} chemical state. The second broad peak observed at 589.45 eV in all the catalysts was due to Cr $2p_{1/2}$ of the Cr^{6+} oxidation state. In BTO_2, an additional less intense peak at 583.88 eV was observed, and this was attributed to Cr $2p_{1/2}$ of Cr^{3+}. The XPS results of Cr-doped $BaTiO_3$ catalysts indicate the presence of Cr in two different oxidation states of 3+ and 6+.

The XPS spectra of oxygen showed a peak at 529.22 eV which corresponds to O 1s in the $BaTiO_3$ lattice[37] (Figure 8e). The XPS spectra of 2.5 and 5 mol % Cr-doped $BaTiO_3$ catalysts synthesized using the MH method is shown in Figure S2a–e. The binding energies of Ba 3d, Ti 2p, Cr 2p, and O 1s are very similar to the CO synthesized Cr-doped $BaTiO_3$ catalysts. The XPS spectrum of BTO_8 for Cr (Figure S2d) indicates that Cr is present in +6 oxidation in which the XPS peak corresponding to +3 (~575 eV) is absent.

3.7. Determination of Acidity Using Pyridine Adsorption. Acidity of the catalysts was determined by pyridine adsorption using FT-IR spectroscopy, and the corresponding FT-IR spectra of all the catalysts are presented in Figure 9a,b and the results are given in Table 5. FT-IR spectra of the catalysts showed bands at 1431 and 1634 cm^{-1}. These were assigned to pyridine chemisorbed to Lewis acid sites on the surface. The amount of Lewis acidity for BTO_1 and BTO_5 (Table 5) was found to be 327 and 329 μmol/g. It indicates that along with improvement in

DOI: 10.1021/acs.inorgchem.6b00240
Inorg. Chem. XXXX, XXX, XXX−XXX

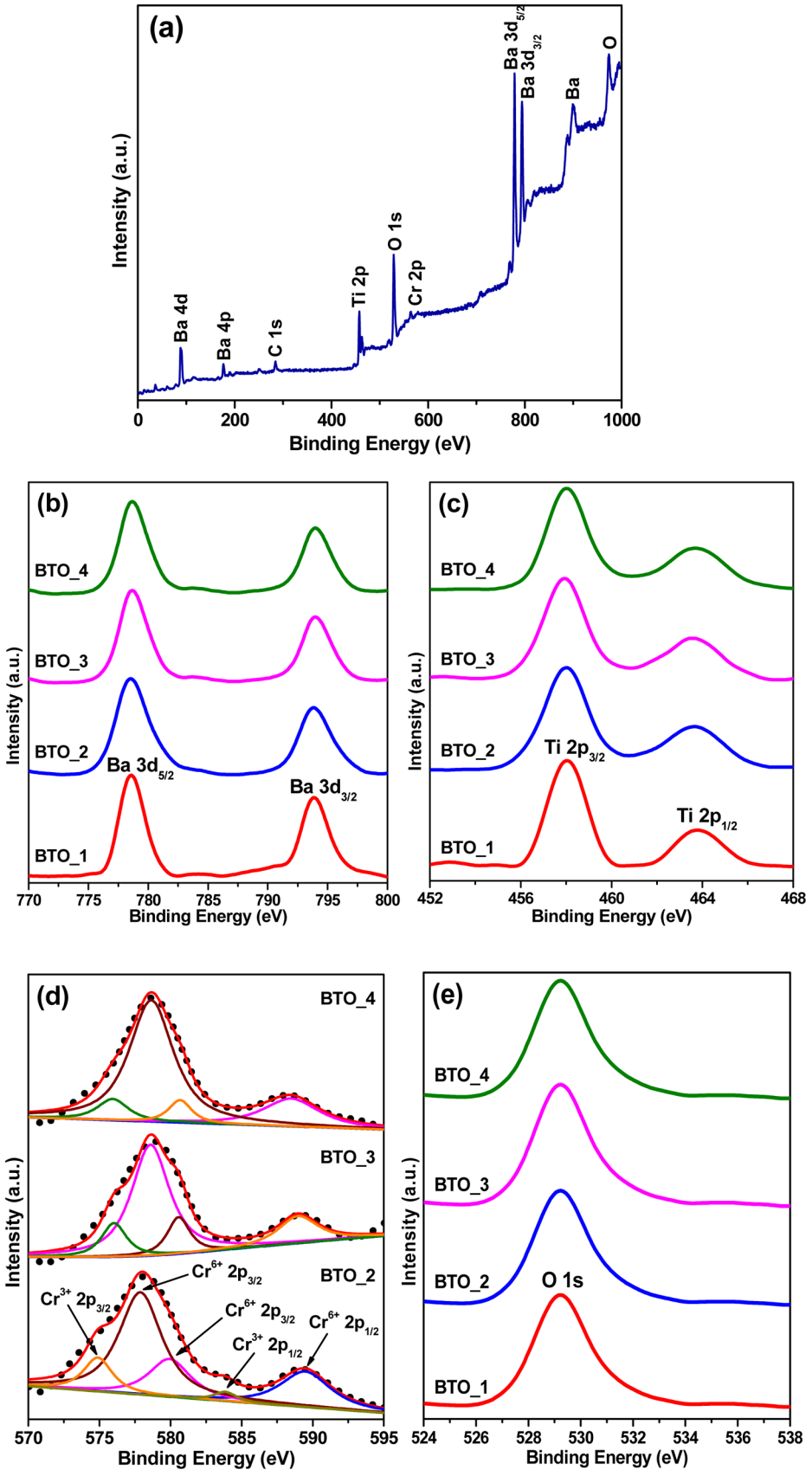

Figure 8. XPS spectra of $BaTiO_3$ and Cr-doped $BaTiO_3$ CO synthesized catalysts: (a) survey spectra of 2.5 mol % Cr-doped $BaTiO_3$, high resolution signals of (b) Ba 3d, (c) Ti 2p, (d) Cr 2p, and (e) O 1s elements.

DOI: 10.1021/acs.inorgchem.6b00240
Inorg. Chem. XXXX, XXX, XXX−XXX

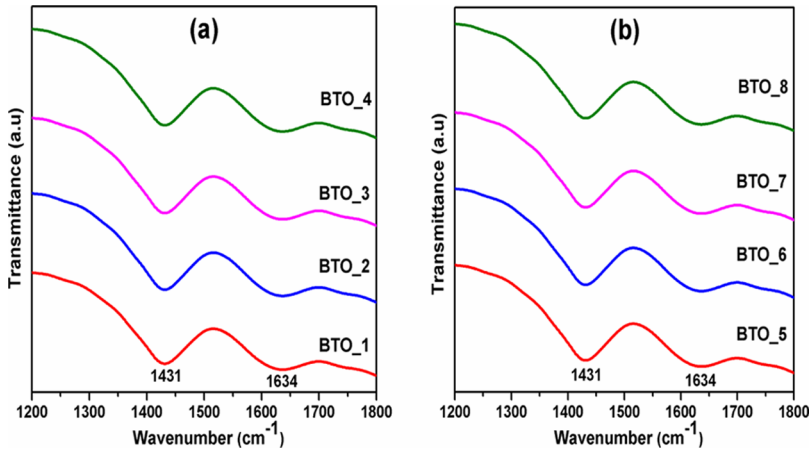

Figure 9. FT-IR spectra of adsorbed pyridine on (a) CO method (b) MH method.

other properties an increase in the number of acid sites was observed in the catalysts synthesized bythe MH method as compared to CO method, and it has been also observed that the amount of Lewis acidity increased with an increase in Cr content of all the catalysts.

3.8. Catalytic Hydrogenation of Nitrobenzene. Once the catalysts were thoroughly characterized regarding structure, they were tested as catalysts for the reduction of nitrobenzene to aniline with hydrazine hydrate as the reducing agent. During the course of the reaction, hydrazine hydrate gets converted into hydrogen and nitrogen gas, and the nitrobenzene is reduced to aniline. The influence of various parameters such as temperature, solvents, and catalyst loading was studied for the optimization of the reaction conditions. The details are given in Table 6. Initially

Table 6. Influence of Temperature, Solvent, and Catalyst Loading on Aniline Yield[a]

sr. no.	catalyst (mg)	hydrazine hydrate (mmol)	solvent	temp (°C)	yield (%)
1	80	30	2-propanol	40	10
2	80	30	2-propanol	60	45
3	**80**	**30**	**2-propanol**	**80**	**100**
4	80	30	methanol	80	50
5	80	30	ethanol	80	75
6	80	30	ACN	80	46
7	80	30	DMSO	80	20
8	80	30	THF	80	12
9	80	30	toluene	80	5
10	60	30	2-propanol	80	55
11	40	30	2-propanol	80	<20
12	0	30	2-propanol	80	0
13	80	20	2-propanol	80	68
14	80	10	2-propanol	80	19

[a]Reaction conditions: Nitrobenzene (10 mmol), hydrazine hydrate (30 mmol), KOH (10 mmol) solvent (10 mL) for 3 h. catalyst BTO_3. [b]GC yield.

80 mg of BTO_3 catalyst was used for optimizing the temperature and solvent. It was found that 99.7% of the aniline product was formed at 80 °C in 3 h. The temperature below 80 °C lowers the aniline yield. 2-Propanol was found to be the best solvent after screening various solvents. It was also interesting to note that the 75% yield of the product was obtained in ethanol medium. The catalyst loading of 80 mg was sufficient to give a maximum yield of the required product. In the absence of either catalyst or KOH, there was no reaction.

The activity of catalysts prepared by CO and MH methods was compared and is shown in Table 7. It can be seen from the table that the CO synthesized BTO catalyst (BTO_1) shows less nitrobenzene conversion and aniline yield. To increase the conversion of nitrobenzene and to achieve maximum aniline yield, Cr was doped into the BTO catalyst and tested for catalytic reduction of nitrobenzene. It was observed that conversion of nitrobenzene has been improved with an increase in Cr content up to 2.5% (BTO_3) and remains constant with a further increase in Cr content to 5% (BTO_4). The increase in conversion with Cr content in the catalysts could be due to an increase in Lewis acidity, although the particle size and BET surface area of the catalysts decreased due to agglomeration of particles with Cr content in the catalysts. The BTO catalyst (BTO_5) synthesized via the MH method itself is very active and showed a maximum nitrobenzene conversion of 99.3% with 98.2% aniline yield. It was observed from the reaction conducted on Cr-doped BTO MH catalysts (BTO_6 to BTO_8) that the conversion remained constant with a slight decrease in the aniline yield. This was due to formation of byproducts such as azobenzene and azoxybenzene during the reaction via condensation path.[21] From the above results it was found that the Cr content in BTO facilitates reduction in a shorter time compared to pure BTO catalysts synthesized via CO and MH methods. The reason being MH synthesized BTO (BTO_5) itself highly active compared to CO synthesized BTO catalyst (BTO_1) could be due to improved properties of reduced particle size high surface area and pore volume of the catalyst (Table 3), because of microwave heating.

To study the scope and applicability of the developed protocol using hydrazine hydrate, reactions of various substituted nitrobenzene were investigated. Since the reduction of nitrobenzene to aniline was maximum on BTO_3, reduction of several nitro aromatics was carried out on this catalyst (Table 8). Excellent yields of desired products were obtained with substituted nitrobenzene. It can be seen that the *ortho* substituted compounds showed less yield compared to *para* substituted compounds which might be attributed to steric hindrance. In the case of 1 chloro, 2, 4 dinitrobenzene selectively one nitrogroup was reduced leading to the formation of 1 chloro, 2, nitrobenzene 4 amine. Yields were determined by GC-FID and compared with authentic samples. Quantitative and qualitative analysis of all amines were made by GC and GC−MS and identified by comparison with authentic samples.

Catalyst Reusability. For the study of the reusability BTO_3 and BTO_7 catalysts were chosen for comparison purposes.

DOI: 10.1021/acs.inorgchem.6b00240
Inorg. Chem. XXXX, XXX, XXX−XXX

Table 7. Catalytic Reduction of Nitrobenzene to Aniline Conducted over CO and MH Catalysts[a]

entry	catalyst	reaction time (h)	NB conversion (%)	sel. to AN (%)	sel. to AZ (%)[b]	sel. to AZY (%)[c]	yield of AN (%)
1	BTO_1	6	80.1	96.3		3.56	77.1
2	BTO_2	3	88.3	100			88.3
3	BTO_3	3	99.9	99.7		0.273	99.7
4	BTO_4	3	99.9	99.8		0.157	99.8
5	BTO_5	6	99.3	98.9	1.05	0.17	98.2
6	BTO_6	3	99.9	92.5	0.90	6.57	92.4
7	BTO_7	3	99.0	93.8	1.02	4.18	92.8
8	BTO_8	3	99.0	91.3	1.15	7.57	90.4

[a]Reaction conditions: nitrobenzene (10 mmol), KOH pellets (10 mmol), N_2H_4 (30 mmol), catalyst (80 mg), and 2-propanol (10 mL), refluxed for 2−6 h at 80 °C. [b]Azobenzene (AZ). [c]Azoxybenzene (AZY).

Table 8. Catalytic Reduction of Various Aromatic Nitro Compounds with BTO_3 Catalyst[a]

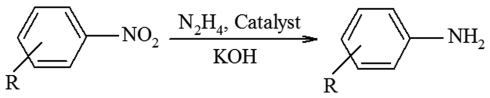

entry	substrate, R	time (h)	NB conversion (%)	AN, yield (%)
1	1-Cl, 2,4-NO_2	6	100	68.2
2	3-NO_2	6	100	72.6
3	4-OCH_3	3	77.3	77.3
4	2-OCH_3	12	30	30
5	2-CH_3	12	99	80.0
6	4-CH_3	4	100	100
7	2-NH_2	2	100	100
8	2-OH	4	100	100
9	4-OH	3	100	100

[a]Reaction conditions: Substrate (10 mmol), KOH pellets (10 mmol), N_2H_4 (30 mmol) catalyst (80 mg) and 2-propanol/Ethanol (10 mL), reflux for 2−6 h at 80 °C.

Table 9. Recyclability of BTO_3 and BTO_7 for Catalytic Reduction of Nitrobenzene

catalyst	cycle	aniline yield (%)	reaction time (h)
BTO_3	1	100	3
	2	100	3
	3	100	4
	4	100	4.2
	5	92	6
BTO_7	1	92	3
	2	92.6	3
	3	92	3
	4	90	4
	5	85	5

It has been observed that the catalyst could be used up to four times without any loss in the activity; however, product yield decreased after four cycles.

4. CONCLUSIONS

Cr-doped $BaTiO_3$ catalysts were successfully synthesized by using conventional oxalate and microwave assisted hydrothermal methods. X-ray diffraction studies and Rietveld refinement results indicate that $BaTi_{1-x}Cr_xO_3$ catalysts synthesized by the oxalate method crystallized in a tetragonal $BaTiO_3$ structure with *P4mm* space group along with trace amounts of impurities corresponding to titanium oxide, barium carbonate, and chromium oxide, whereas microwave synthesized catalysts were crystallized in pure cubic $BaTiO_3$ structure with $Pm\bar{3}m$ space group without any trace of impurities. The particle size of the microwave synthesized catalysts deduced from TEM images is less compared to conventional oxalate catalysts and in the range of 20−30 nm. XPS analysis revealed that the Cr is present in 3+ and 6+ oxidation states in all the catalysts. Microwave synthesized catalysts showed a 4−10-fold increase in surface area and pore volume compared to oxalate synthesized catalysts. Catalytic reduction of nitrobenzene to aniline studies reveal that microwave synthesized $BaTiO_3$ itself is active and showed 99.3% nitrobenzene conversion with 98.2% aniline yield, whereas $BaTiO_3$ synthesized by the conventional oxalate method showed only 80.1% nitrobenzene conversion with 77.1% aniline yield. Cr-doping into $BaTiO_3$ lattice facilitates the reaction in a short time in all the catalysts, and its effect is particularly notable in oxalate synthesized catalysts by achieving 99.9% nitrobenzene conversion with 99.7% aniline yield on 2.5 mol % Cr-doped $BaTiO_3$. The increase in conversion was due to increase in Lewis acidity with Cr content in the catalysts. From the above results it was concluded that the Cr-doped $BaTiO_3$ nanocatalysts containing high surface area, pore volume, and reduced particle size with good dispersion and with high catalytic activity is successfully obtained in less time using the microwave assisted hydrothermal synthesis method. The present study reveals that the microwave hydrothermal synthesis method would be an interesting energy efficient technology to explore for the synthesis of various nanomaterials in their pure form in order to achieve better physiochemical and catalytic properties of the materials.

■ ASSOCIATED CONTENT

Supporting Information

The Supporting Information is available free of charge on the ACS Publications website at DOI: 10.1021/acs.inorgchem.6b00240.

Rietveld refinement patterns for BTO_3, BTO_4, BTO_7, and BTO_8 is given in Figure S1, and XPS spectra of BTO_7 and BTO_8 catalysts given in Figure S2 (PDF)

■ AUTHOR INFORMATION

Corresponding Author

*E-mail: ch.srilakshmi@sscu.iisc.ernet.in.

Notes

The authors declare no competing financial interest.

■ ACKNOWLEDGMENTS

This work was financially supported by Department of Science and Technology (DST) India through INSPIRE project. C.S.L. would like to thank Prof. Ramasesha for the support of this work.

DOI: 10.1021/acs.inorgchem.6b00240
Inorg. Chem. XXXX, XXX, XXX−XXX

REFERENCES

(1) Farhadi, S.; Siadatnasab, F. *J. Mol. Catal. A: Chem.* **2011**, *339*, 108−116.
(2) Peña, M. A.; Fierro, J. L. G. *Chem. Rev.* **2001**, *101*, 1981−2018.
(3) Mathews, S.; Ramesh, R.; Venkatesan, T.; Benedetto, J. *Science* **1997**, *276*, 238−240.
(4) Yoo, J. H.; Gao, W.; Yoon, K. H. *J. Mater. Sci.* **1999**, *34*, 5361−5369.
(5) Feteira, A.; Sinclair, D. C.; Reaney, I. M.; Somiya, Y.; Lanagan, M. T. *J. Am. Ceram. Soc.* **2004**, *87*, 1082−1087.
(6) Smith, B. M.; Page, K.; Siegrist, T.; Redmond, P. L.; Walter, E. C.; Seshadri, R.; Brus, L. E.; Steigerwald, M. L. *J. Am. Chem. Soc.* **2008**, *130*, 6955−6963.
(7) Zhang, Y.; Chen, C.; Gao, R.; Xia, F.; Li, Y.; Che, R. *Appl. Phys. Lett.* **2015**, *107*, 182902−182905.
(8) Farhadi, S.; Momeni, Z.; Taherimehr, M. *J. Alloys Compd.* **2009**, *471*, L5−L8.
(9) Sasirekha, N.; Rajesh, B.; Chen, Y. W. *Ind. Eng. Chem. Res.* **2008**, *47*, 1868−1875.
(10) Vaidyanathan, B.; Raizada, P.; Rao, K. J. *J. Mater. Sci. Lett.* **1997**, *16*, 2022.
(11) Gibbsons, K. E.; Jones, M. O.; Blundell, S. J.; Mihut, A. I. *Chem. Commun.* **2000**, 159−160.
(12) Rappoport, Z. *The Chemistry of Anilines*; John Wiley and Sons: England, U.K., 2007.
(13) Trost, B. M.; Fleming, I. *Comprehensive Organic Synthesis: Selectivity, Strategy, and Efficiency in Modern Organic Chemistry*; Pergamon Press: Oxford, U.K., 1991.
(14) Brown, C. A. *J. Org. Chem.* **1970**, *35*, 1900−1904.
(15) Machado, B. F.; Morales-Torres, S.; Pérez-Cadenas, A. F.; Maldonado-Hódar, F. J.; Carrasco-Marín, F.; Silva, A. M. T.; Figueiredo, J. L.; Faria, J. L. *Appl. Catal., A* **2012**, *425-426*, 161−169.
(16) Palomares, A. E.; Franch, C.; Yuranova, T.; Kiwi-Minsker, L. K.; García-Bordeje, E. G.; Derrouiche, S. *Appl. Catal., B* **2014**, *146*, 186−191.
(17) Yan, M.; Jin, T.; Chen, Q.; Ho, H. E.; Fujita, T.; Chen, L. Y.; Bao, M.; Chen, M. W.; Asao, N.; Yamamoto, Y. *Org. Lett.* **2013**, *15*, 1484−1487.
(18) Tejuca, L. G.; Fierro, J. L. G.; Tascon, J. M. D. *Adv. Catal.* **1989**, *36*, 237−328.
(19) Kremenic, G.; Nieto, J. M. L.; Tascón, J. M. D.; Tejuca, L. G. *J. Chem. Soc., Faraday Trans. 1* **1985**, *81*, 939−949.
(20) Wu, Y.; Yu, T.; Dou, B.; Wang, C.; Xie, X.; Yu, Z.; Fan, S.; Fan, Z.; Wang, L. *J. Catal.* **1989**, *120*, 88−107.
(21) Srilakshmi, C.; Mohan Rao, G.; Saraf, R. *RSC Adv.* **2015**, *5*, 45965−45973.
(22) Janousch, M.; Meijer, G. I.; Staub, U.; Delley, B.; Karg, S. F.; Andreasson, B. P. *Adv. Mater.* **2007**, *19*, 2232−2235.
(23) Zhu, J.; Deng, Z.; Chen, F.; Zhang, J.; Chen, H.; Anpo, M.; Huang, J.; Zhang, L. *Appl. Catal., B* **2006**, *62*, 329−335.
(24) Sharma, R. K.; Bhatnagar, M. C.; Sharma, G. L. *Sens. Actuators, B* **1997**, *45*, 209−215.
(25) Thirupathi, B.; Smirniotis, P. G. *Appl. Catal., B* **2011**, *110*, 195−206.
(26) Ahmed, O. S.; Dutta, D. K. *J. Mol. Catal. A: Chem.* **2005**, *229*, 227−231.
(27) Panda, A. K.; Mishra, B. G.; Mishra, D. K.; Singh, R. K. *Colloids Surf., A* **2010**, *363*, 98−104.
(28) Ganguly, M.; Rout, S. K.; Ahn, C. W.; Kim, I. W.; Kar, M. *Ceram. Int.* **2013**, *39*, 9511−9524.
(29) Chen, C. L.; Shen, J.; Chen, S. Y.; Luo, G. P.; Chu, C. W.; Miranda, F. W.; Van Keuls, J. C.; Meletis, E. I.; Chang, H.; Jiang, J. C. *Appl. Phys. Lett.* **2001**, *78*, 652−654.
(30) García-Hernández, M.; García-Murillo, A.; Carrillo-Romo, F. d. J.; Jaramillo-Vigueras, D.; Chadeyron, G.; De la Rosa, E. D. L.; Boyer, D. *Int. J. Mol. Sci.* **2009**, *10*, 4088−4101.
(31) Wang, J.; Ding, S. W.; Lv, S. F. *Indian J. Chem, Sec A* **2008**, *47*, 1365−1368.
(32) Nayak, S.; Sahoo, B.; Chaki, T. K.; Khastgir, D. *RSC Adv.* **2014**, *4*, 1212−1224.
(33) Wei, C. Y.; Kuo, S. H.; Hung, Y. M.; Huang, W. C.; Adriyanto, F.; Wang, Y. H. *IEEE Electron Device Lett.* **2011**, *32*, 90−92.
(34) Wegmann, M.; Watson, L.; Hendry, A. *J. Am. Ceram. Soc.* **2004**, *87*, 371−377.
(35) Yao, Z.; Liu, H.; Liu, Y.; Wu, Z.; Shen, Z.; Liu, Y.; Cao, M. *Mater. Chem. Phys.* **2008**, *109*, 475−481.
(36) Zhang, J.; Xie, K.; Wei, H.; Qin, Q.; Qi, W.; Yang, L.; Ruan, C.; Wu, Y. *Sci. Rep* 2014, *4*, 7082−1−7082−14.
(37) Wang, R. X.; Zhu, Q.; Wang, W. S.; Fan, C. M.; Xu, A. W. *New J. Chem.* **2015**, *39*, 4407−4413.

DOI: 10.1021/acs.inorgchem.6b00240
Inorg. Chem. XXXX, XXX, XXX−XXX